International Journal of Heat and Mass Transfer 102 (2016) 1230–1244

Contents lists available at ScienceDirect

International Journal of Heat and Mass Transfer

journal homepage: www.elsevier.com/locate/ijhmt

Numerical estimation of convective heat transfer coefficient through linearization

Fermín S.V. Bazán [a,*,1], Luciano Bedin [a,1], Fabio Bozzoli [b]

[a] Department of Mathematics, Federal University of Santa Catarina, 88040-900 Florianópolis, SC, Brazil
[b] Department of Industrial Engineering, University of Parma, Parco Area delle Scienze 181/A, I-43124 Parma, Italy

ARTICLE INFO

Article history:
Received 23 December 2015
Received in revised form 30 June 2016
Accepted 5 July 2016

Keywords:
Inverse heat transfer
Coiled tubes
Chebyshev pseudospectral methods
Regularization
Discrepancy principle

ABSTRACT

In this work, methods for estimating the local convective heat transfer coefficient in coiled tubes are proposed and assessed. The methods include truncated generalized singular value decomposition, Tikhonov regularization, and a novel filtering technique which mitigates noise propagation by truncating the frequency content of differentiation matrix operators. Numerical results on synthetic and experimental data are reported to illustrate the effectiveness of the methods. Synthetic data resemble well experimental data often encountered in technical applications and may be useful in the assessment of numerical methods and in the design of coiled tube heat exchangers. The success of the methods is supported by both an efficient solver for the forward problem based on a highly accurate pseudospectral method and a proper selection of regularization parameters.

1. Introduction

The estimation of local heat transfer coefficient over a given domain has become important in several industrial applications such as food processing, nuclear power production, air-conditioning systems and power electronics, among others [12,34,35]. In particular, because coiled tubes cause heat transfer enhancement, the development of estimation techniques of heat transfer coefficient has attracted the attention of many researchers [7,12,14,31,32]. Coils induce an irregular heat transfer coefficient distribution along the wall perimeter that may be critical in some industrial applications. However, most of research papers presents results only in terms of thermal performance averaged along the wall circumference, due to the practical difficulty of measuring heat flux in the inner wall surface of a pipe. Placing probes in a pipe is usually infeasible because of the perturbation effects of the probes on the observed phenomenon, the geometric inaccessibility of the surface, or because of the fluid in the pipe that may destroy the sensors.

A way to circumvent the above difficulty is to estimate the heat transfer coefficient from the solution of an inverse heat conduction problem (IHCP) based on temperature measurements on the external tube wall surface and a mathematical model that describes the physics involved. The application of IHCP solution techniques becomes interesting as the experimental problem of monitoring heat transfer on the internal tube wall is avoided. However, solving IHCPs is not as easy as one would wish and complications take place because this class of problems are generally ill-posed [9]. As a result, the problem solution, when it exists, may not be unique and may be very sensitive to small variations in the input data. A way to bypass the ill-posedness of IHCPs is through the use of regularization methods. Efforts in this direction have been done by Bozzoli et al. in a number of works as follows: in [12,14] where Tikhonov regularization is employed, in [13] where temperature data is processed by a filtering technique in order to obtain estimates of the heat transfer coefficients under a small tube thickness assumption, and in [11] where Tikhonov Regularization Method is compared with a Gaussian Filtering Technique. Besides Tikhonov regularization-based methods, the most popular methods include Alifanov's iterative regularization method [1,28], function specification methods [9,29], and methods based on filtering properties [15,18,27]. Related contributions are also encountered in several places. Bai et al. [2] experimentally studied the turbulent heat transfer in helically coiled tubes. Xu and Chen [39] discuss a nonlinear problem of determining the heat transfer coefficient in two-phase flow in an inclined tube by building a steady-state two-dimensional heat conduction model. Martin and Dulikravich [19] describe an inverse boundary element method (BEM) for determining the heat transfer coefficients on

* Corresponding author.
E-mail addresses: fermin@mtm.ufsc.br (F.S.V. Bazán), luciano.bedin@ufsc.br (L. Bedin), fabio.bozzoli@unipr.it (F. Bozzoli).

[1] The work of both authors was supported by CNPq, Brazil, Grant 477093/2011-6.

http://dx.doi.org/10.1016/j.ijheatmasstransfer.2016.07.021
0017-9310/

Nomenclature

Symbol	Quantity, SI unit
B_i	Biot number
h	convective heat-transfer coefficient, W/m^2 K
$\mathbf{J}$	sensitivity matrix, K/W
k	truncation parameter
Q	heat flux, W/m^2
$\mathbf{Q}$	heat flux vector, W/m^2
q_g	internal heat generation per unit volume, W/m^3
r	radial coordinate, m
$\mathbf{R}$	residual vector, K
T	temperature, K
$\mathbf{T}$	temperature vector, K
$\widetilde{\mathbf{T}}$	experimental temperature vector, K
α	overall heat transfer coefficient, W/m^2 K
ϵ	noise, K
ϕ	angular coordinate, rad
λ_w	thermal conductivity, W/m K
λ	regularization parameter, K m^2/W
Ψ	product function, K W/m^2

Subscripts, superscripts	
b	bulk
env	environment
E	external
I	internal
Acronym	Meaning
CPS	Chebyshev pseudospectral method
DP	discrepancy principle
FP	fixed point method
FDMA	filtering via differentiation matrix approach
GSVD	generalized singular value decomposition
LC	L-curve
MPR	minimum product rule
OPT	minimum normwise relative error
SVD	singular value decomposition
TGSVD	truncated generalized singular value decomposition
TRM	Tikhonov regularization method
TSVD	truncated singular value decomposition

solid surfaces of arbitrary shape; BEM-based methods also are employed in [33,41]; a three-dimensional inverse identification model for the heat transfer coefficient was introduced in [40] and solved using sensitivity analysis. Hybrid schemes that combine Laplace transform, finite difference and least-squares methods to estimate time and space-wise dependent heat transfer coefficient in rectangular domains are addressed via linearization in [16,17]. Lu et al. [25] implemented an estimation approach based on the IHCP solution, using the conjugate gradient method, to estimate the unknown transient fluid temperatures near the inner wall in section of a pipe elbow with thermal stratification. Su and Hewitt [37] estimated the time-dependent heat transfer coefficient of forced convective flow boiling over the outer surface of a heater tube solving an inverse heat conduction problem based on Alifanov's iterative regularization method. Rouizi et al. [36] employed the Quadrupole method to retrieve the temperature and flux distributions over the internal surface of a micro-channel using temperature profiles measured at the external surface in conjunction with the truncated singular value decomposition (TSVD) method as regularization technique.

In this paper, the research work by Bozzoli et al. [12–14] is investigated further and new methods are proposed for estimating the heat transfer coefficient in coiled tubes. In particular, in Section 2, a benchmark solution problem is introduced, which resembles experimental temperature measurements often found in technical applications, see, e.g., Bozzoli et al. [12], and can be useful in the assessment of numerical methods for estimating heat transfer coefficient. In Section 3, a comprehensive and simple approach for the direct problem is proposed based on a highly accurate pseudospectral method. Proceeding in this way, the calculation of preliminary quantities such as the sensitivity matrix, necessary for the Tikhonov regularization method to work, becomes clear and easy to follow from the computational point of view. In Section 4, in addition to describing several existing methods for estimating the heat transfer coefficient in IHCPs, a novel estimation method is proposed following the same spirit as the filtering technique described in [13,11]; the novelty here is that no optimization problem is solved. Finally, in Section 5, all estimation techniques are evaluated by applying them to synthetic data obtained from the proposed benchmark solution as well as to experimental data obtained by Bozzoli et al. in [12]; the paper ends with some concluding remarks in Section 6.

2. Mathematical model and benchmark solution

All estimation procedures in this study depend on the assumption that the heat transfer coefficient is embedded in a 2D mathematical model of a selected cross-section of a coiled tube, as shown schematically in Fig. 1, under the laminar flow regime as done by Bozzoli et al. [12] and Rainieri et al. [31] in their experimental investigations. In cases like this, uniform heating is generated by dissipating a heat flux using the Joule effect directly within the tube wall. Without additional assumptions, the 2D direct heat conduction problem in polar coordinates (r, ϕ) is expressed in the form:

$$\lambda_w \frac{1}{\mathrm{r}} \frac{\partial}{\partial \mathrm{r}} \left(\mathrm{r} \frac{\partial T}{\partial \mathrm{r}} \right) + \lambda_w \frac{1}{\mathrm{r}^2} \frac{\partial^2 T}{\partial \phi^2} + q_g = 0, \quad 0 < \mathrm{r_I} < \mathrm{r} < \mathrm{r_E},\ 0 \leqslant \phi \leqslant 2\pi, \tag{1}$$

$$\lambda_w \frac{\partial T}{\partial \mathrm{r}}(\mathrm{r_E}, \phi) = \alpha (T_{\mathrm{env}} - T(\mathrm{r_E}, \phi)), \quad 0 \leqslant \phi \leqslant 2\pi, \tag{2}$$

$$-\lambda_w \frac{\partial T}{\partial \mathrm{r}}(\mathrm{r_I}, \phi) = h(\phi)(T_b - T(\mathrm{r_I}, \phi)), \quad 0 \leqslant \phi \leqslant 2\pi. \tag{3}$$

Physically, q_g denotes the heat generated by the Joule effect in the wall, $\mathrm{r_I}, \mathrm{r_E}$ denote the internal and external radius of the cross section of the tube, respectively, λ_w denotes the wall thermal conductivity, α denotes the reciprocal of the overall heat transfer resistance between the tube wall and the surrounding environment with temperature T_{env}, $h(\phi)$ denotes the convective heat transfer coefficient at the fluid-internal wall interface, and T_b denotes the bulk-fluid temperature on the test section.

In the inverse estimation problem of interest, the convective transfer coefficient $h(\phi)$ is regarded as unknown and must be estimated from measured temperature values as input data: $\widetilde{T}_j = T(\mathrm{r_E}, \phi_j) + \varepsilon_j, j = 1, \ldots, M$, where $T(\mathrm{r_E}, \phi)$ is assumed to match (1)–(3) and ε_j denotes random noise. It is worth noticing that due to the boundary condition (3), this estimation problem should be handled by an appropriate nonlinear optimization technique because $h(\phi)$ does not depend linearly on T. An approach which circumvents possible difficulties often encountered when dealing

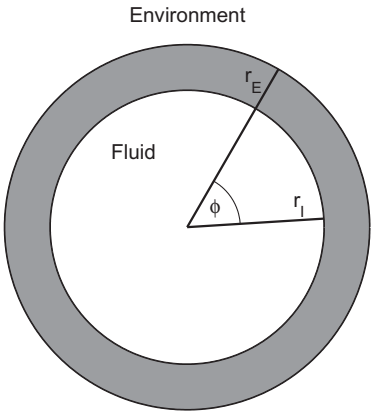

Fig. 1. Geometrical domain.

with non linear problems replaces the boundary condition (3) with one that transforms the original problem into a linear estimation problem. In fact, introducing

$$-\lambda_w \frac{\partial T}{\partial r}(r_I, \phi) = Q(\phi), \tag{4}$$

where $Q(\phi)$ stands for the heat-flux distribution at the fluid-wall interface, one can consider the more tractable problem that estimates $Q(\phi)$ from measured data $\widetilde{T}(r_E, \phi_i)$ instead. The reason is that the heat-flux distribution $Q(\phi)$ can be proved to depend linearly on T [9]. Once the heat-flux distribution is estimated, the convective heat-transfer coefficient can be estimated as

$$h(\phi) = \frac{Q(\phi)}{T_b - T(r_I, \phi)}, \tag{5}$$

where $T(r_I, \phi)$ is the temperature distribution at the internal tube wall estimated by solving the direct problem (1)–(3) with (3) being replaced by the boundary condition (4), where $Q(\phi)$ is the estimated heat-flux distribution. This approach has been proved successful in [12] and it will be used in this work as well, with $Q(\phi)$ being estimated in several ways and methods.

For comparison purposes all estimation methods in this investigation will be tested and assessed by using a test problem with exact solution satisfying (1), (2) and (4) for prescribed heat flux Q. To generate such test problem we look for solutions of (1) described by

$$T(r, \phi) = f(r) + V(r, \phi), \tag{6}$$

where $f(r)$ is a radial solution of the nonhomogeneous problem (1)

$$(rf')' = -\frac{q_g r}{\lambda_w} \tag{7}$$

and $V(r, \theta)$ is a solution of the homogeneous partial differential equation (PDE)

$$\lambda_w \frac{1}{r}\frac{\partial}{\partial r}\left(r\frac{\partial V}{\partial r}\right) + \lambda_w \frac{1}{r^2}\frac{\partial^2 V}{\partial \phi^2} = 0. \tag{8}$$

Now, it can be readily seen that the general solution of (7) is

$$f(r) = \frac{-q_g r^2}{4\lambda_w} + F\ln(r) + G, \tag{9}$$

where F and G are arbitrary constants. On the other hand, following the standard separation of variables method, see, e.g., [22], we can find infinitely many solutions of the homogeneous problem (8). Indeed, by looking for product solutions of the form $V(r, \phi) = X(r)Y(\phi)$, it can be seen that the product form will satisfy the PDE if

$$Y''(\phi) + \gamma^2 Y(\phi) = 0, \quad 0 \leqslant \phi \leqslant 2\pi, \tag{10}$$

$$r^2 X''(r) + rX'(r) - \gamma^2 X(r) = 0, \quad r_I < r < r_E, \tag{11}$$

where γ is an eigenvalue of (10). Taking into account that physical solutions of (10) must be 2π-periodic, routine calculations show that the eigenvalues are $\gamma_n = n, n = 0, 1, 2, \ldots$, with respective eigen solutions given by $\{C_n\cos(n\phi), D_n\sin(n\phi)\}$, where C_n, D_n are arbitrary constants. Inserting $\gamma = n$ into the Cauchy–Euler equation (11), it can seen that the associated general solution are $X_0(r) = A_0\ln(r) + B_0$ and $X_n(r) = A_n r^n + \frac{B_n}{r^n}$. Since the PDE (8) is linear, the superposition principle, (6) and (9) show that the general solution for (1) can be described as

$$T(r, \phi) = \frac{-q_g r^2}{4\lambda_w} + A_0 + C_0\ln(r) + \sum_{n=1}^{\infty}(A_n r^n + C_n r^{-n})\cos(n\phi) + \sum_{n=1}^{\infty}(B_n r^n + D_n r^{-n})\sin(n\phi), \tag{12}$$

where the arbitrary constants have been conveniently relabeled. Note that $T(r, \phi)$ in (12) does not satisfy (2) and (4). This shows that the construction of exact solutions for the model described by (1), (2) and (4) for prescribed $Q(\phi)$, requires the determination of constants which are difficult to calculate. Thus, for simplicity, all estimation methods in this investigation will be tested and assessed by using a benchmark solution for (1), (2) and (4) which involves just the Fourier mode $X_1(r)\cos(\phi)$:

$$T(r, \phi) = \frac{-q_g(r^2 - r_E^2)}{4\lambda_w} + A\ln\left(\frac{r}{r_E}\right) + B + C\cos(\phi)\left(r + \frac{D}{r}\right), \tag{13}$$

where A, B, C, D are suitably chosen constants. The motivation for choosing such solution is that appropriate constants A, B, C, D lead to temperature distributions that resemble experimental data reported in [12]. It remains to select A, B, C, D such that the boundary condition (2) is also satisfied. In fact, enforcing $T(r, \phi)$ to satisfy the boundary condition (2) it follows

$$\lambda_w\left(\frac{-q_g r_E}{2\lambda_w} + \frac{A}{r_E} + C\cos(\phi)\left(1 - \frac{D}{r_E^2}\right)\right) = \alpha T_{env} - \alpha\left(B + C\cos(\phi)\left(r_E + \frac{D}{r_E}\right)\right).$$

Equating constant and periodic terms leads to

$$\lambda_w\left(1 - \frac{D}{r_E^2}\right) = -\alpha\left(r_E + \frac{D}{r_E}\right), \tag{14}$$

and

$$\lambda_w\left(\frac{-q_g r_E}{2\lambda_w} + \frac{A}{r_E}\right) = \alpha T_{env} - \alpha B. \tag{15}$$

That is,

$$D = \frac{r_E^2(\lambda_w + \alpha r_E)}{\lambda_w - \alpha r_E}, \quad A = \frac{q_g r_E^2}{2\lambda_w} + \frac{r_E}{\lambda_w}\alpha(T_{env} - B). \tag{16}$$

Thus, infinitely many benchmark solutions can be constructed by selecting parameters B and C. For instance, for $B = T_{env}$ and arbitrary C the benchmark solution becomes

$$T(r, \phi) = \frac{-q_g(r^2 - r_E^2)}{4\lambda_w} + \frac{q_g}{2\lambda_w} r_E^2\ln\left(\frac{r}{r_E}\right) + T_{env} + C\cos(\phi)\left(r + \frac{D}{r}\right),$$

with D given in (16). Finally, note that regardless the choice of constants B, C, if the heat-flux distribution $Q(\phi)$ is defined by the boundary condition (4) with $T(r, \phi)$ given in (13):

$$Q(\phi) = -\lambda_w \left.\frac{\partial T(r, \phi)}{\partial r}\right|_{r=r_I} = \frac{q_g r_I}{2} - \lambda_w\frac{A}{r_I} - \lambda_w C\cos(\phi)\left(1 - \frac{D}{r_I^2}\right), \tag{17}$$

then $T(\mathrm{r},\phi)$ constructed in this way satisfies the model (1), (2), (4). The most important consequence of the above constructive process is that it delivers an exact solution that can be used for testing and assessing numerical methods for estimating the heat transfer coefficient $h(\phi)$ based on prior estimation of $Q(\phi)$ as described in (5).

3. Efficient numerical method for the forward problem

This section introduces a highly accurate numerical method for problem described by (1), (2) and (4), based on the Chebyshev pseudospectral (CPS) collocation approach for partial differential equations (PDEs). The CPS approach has become an efficient way to solve approximately partial differential equations (PDEs), see, e.g., [20,30,38], due to its high accuracy and relatively lower computation cost compared to other methods, and is particularly important when solving IHCPs since, as we will see, the forward problem has to be solved efficiently many times. Roughly speaking, the CPS approach constructs the approximate solution in a space of algebraic polynomials of degree N so that the differential equation being solved is satisfied in a specified number of points x_j called collocation points. If the problem is unidimensional on a bounded interval, for instance, and the approximate solution is denoted by U_N and expressed in Lagrangian form

$$U_N(x) = \sum_{k=0}^{N} U_k \ell_k(x), \tag{18}$$

where $U_j \doteq U_N(x_j)$, $j = 0, 1, \ldots, N$, and where $\ell_k(x)$ denotes the Lagrangian polynomial, then the coefficients U_j become the unknowns of a system of linear equations obtained by discretization of the differential equation, where derivatives of the exact solution $U(x)$ are estimated at the collocation points by differentiating (18) and evaluating the result at the points x_j. Proceeding in this way, with the observation that the pth order derivative of a function f at x_j is denoted by $f^{(p)}(x_j)$, it follows that

$$U_N^{(p)}(x_j) = \sum_{k=0}^{N} U_k \ell_k^{(p)}(x_j), \quad p = 1, 2, \ldots, \tag{19}$$

or in matrix form as

$$\mathrm{U}^{(p)} = D^p \mathrm{U}, \tag{20}$$

where $\mathrm{U} = [U_N(x_0), \ldots, U_N(x_N)]^T$, $\mathrm{U}^{(p)} = [U_N^{(p)}(x_0), \ldots, U_N^{(p)}(x_N)]^T$, and where D is the $(N+1)\times(N+1)$ differentiation matrix whose entries are given by [20,38]

$$D_{j,k} = \ell_k'(x_j), \quad 0 \leqslant j, k \leqslant N. \tag{21}$$

The Chebyshev pseudospectral collocation method takes as collocation points the Chebyshev Gauss–Lobatto points (numbered from left to right) defined by

$$x_j = -\cos\frac{j\pi}{N}, \quad j = 0, 1, \ldots, N. \tag{22}$$

For periodic problems on the interval $[0, 2\pi]$ the pseudospectral collocation method proceeds as before but now with the interpolation polynomial being written using the Fourier basis. This gives rise to a Fourier differentiation matrix which we will denote by $\mathcal{D}$; for details the reader is referred to [30].

In order to apply the CPS approach to the problem of interest it is convenient to map the original domain to the reference domain $[-1, 1]\times[0, 2\pi]$ through the mapping

$$\begin{aligned} \mathrm{r}(r) &= \mathrm{r_I} + \frac{1}{2}(r+1)(\mathrm{r_E} - \mathrm{r_I}), \quad -1 \leqslant r \leqslant 1 \\ \phi(\theta) &= \theta, \quad 0 \leqslant \theta \leqslant 2\pi. \end{aligned} \tag{23}$$

Under the above transformation the boundary value problem of interest becomes

$$\lambda_w\left(\rho^2\frac{\partial^2 T}{\partial \mathrm{r}^2} + \frac{\rho}{\mathrm{r}(r)}\frac{\partial T}{\partial r}\right) + \frac{\lambda_w}{[\mathrm{r}(r)]^2}\frac{\partial^2 T}{\partial \theta^2} + q_g = 0, \quad -1 < r < 1,\ 0 \leqslant \theta \leqslant 2\pi \tag{24}$$

$$\lambda_w \frac{\partial T(1,\theta)}{\partial r} = \frac{\alpha}{\rho}(T_{\mathrm{env}} - T(1,\theta)), \quad 0 \leqslant \theta \leqslant 2\pi \tag{25}$$

$$-\lambda_w \frac{\partial T(-1,\theta)}{\partial r} = \frac{Q(\theta)}{\rho}, \quad 0 \leqslant \theta \leqslant 2\pi \tag{26}$$

where $\rho = 2/(\mathrm{r_E} - \mathrm{r_I})$. The construction of numerical solutions to (24)–(26) via the CPS method starts by considering a mesh consisting of $(N+1)\times M$ grid points on the reference domain based on $(N+1)$ Chebyshev Gauss–Lobatto r_i in the r direction, and M uniformly spaced points $\theta_j = 2\pi j/M, j = 1, \ldots, M$, in the azimuthal direction, under the assumption that the sought solution is periodic with respect to θ and that gridpoints are numbered in lexicographic ordering. This means that partial derivatives in the r direction will be approximated by using the Chebyshev differentiation D, whereas partial derivatives with respect to θ will be approximated by using the $M\times M$ Fourier differentiation matrix $\mathcal{D}$. Partial derivatives in the r direction are approximated as follows. For fixed j let the vector of unknowns be denoted by

$$\overline{T}_j = [T(r_0,\theta_j),\ T(r_1,\theta_j),\ \cdots T(r_N,\theta_j)]^{\mathrm{T}}, \quad j = 1, \ldots, M \tag{27}$$

and let the matrix D be represented in columnwise and row-wise forms

$$D = [d_0\ d_1\ \cdots\ d_N] = [\ell_0\ \cdots\ \ell_N]^{\mathrm{T}} \quad d_i, \ell_i \in \mathbb{R}^{N+1}. \tag{28}$$

Since the second order Chebyshev differentiation matrix, D^2, can be expressed as $D^2 = d_0\ell_0^{\mathrm{T}} + d_1\ell_1^{\mathrm{T}} + \cdots + d_N\ell_N^{\mathrm{T}}$, the second order derivatives of T with respect to r can be approximated as

$$\begin{bmatrix} T_{rr}(r_0,\theta_j) \\ T_{rr}(r_1,\theta_j) \\ \vdots \\ T_{rr}(r_N,\theta_j) \end{bmatrix} \approx D^2 \begin{bmatrix} T(r_0,\theta_j) \\ T(r_1,\theta_j) \\ \vdots \\ T(r_N,\theta_j) \end{bmatrix} = d_0\ell_0^{\mathrm{T}}\overline{T}_j + D_1D_2\overline{T}_j + d_N\ell_N^{\mathrm{T}}\overline{T}_j \tag{29}$$

where

$$D_1 = [d_1\ d_2\ \cdots d_{N-1}], \quad D_2 = [\ell_1\ \cdots\ \ell_{N-1}]^{\mathrm{T}}. \tag{30}$$

Now, since $\ell_i^{\mathrm{T}}\overline{T}_j \approx T_r(r_i,\theta_j)$, the boundary conditions (25) and (26) imply

$$\ell_0^{\mathrm{T}}\overline{T}_j \approx T_r(r_0,\theta_j) = -\frac{Q(\theta_j)}{\rho\lambda_w}, \quad \ell_N^{\mathrm{T}}\overline{T}_j \approx T_r(r_N,\theta_j) = \frac{\alpha}{\rho\lambda_w}(T_{\mathrm{ext}} - T(r_N,\theta_j)). \tag{31}$$

Then, insertion of (31) into (29) shows that the scaled vector of second order derivatives $\lambda_w\rho^2 T_{rr}(r_i,\theta_j)$, $0 \leqslant i \leqslant N, 1 \leqslant j \leqslant M$, can be approximated as

$$\lambda_w\rho^2\begin{bmatrix} T_{rr}(r_0,\theta_j) \\ T_{rr}(r_1,\theta_j) \\ \vdots \\ T_{rr}(r_N,\theta_j) \end{bmatrix} \approx [-\rho\alpha d_N e_{N+1}^{\mathrm{T}} + \lambda_w\rho^2 D_1D_2]\overline{T}_j - \rho Q_j d_0 + \rho\alpha T_{\mathrm{ex}} d_N \tag{32}$$

where e_i denotes the ith unit vector in $\mathbb{R}^{N+1}$ and $Q_j \doteq Q(\theta_j)$. Similarly, the scaled vector of first order derivatives $\frac{\lambda_w\rho}{r_i}T_r(r_i,\theta_j)$ can be approximated as

$$\lambda_w\rho\begin{bmatrix}\frac{1}{r_0}T_r(r_0,\theta_j)\\ \frac{1}{r_1}T_r(r_1,\theta_j)\\ \vdots\\ \frac{1}{r_N}T_r(r_N,\theta_j)\end{bmatrix}\approx\lambda_w\rho\,\mathsf{R}^{-1}D\overline{T}_j\;=\check{D}\overline{T}_j-\check{Q}_j \tag{33}$$

where

$$\mathsf{R}=\mathrm{diag}(\mathsf{r}_0,\ldots,\mathsf{r}_N),\quad \check{Q}_j=\mathsf{R}^{-1}\left(Q_je_1-\alpha T_{ex}e_{N+1}\right),\quad \check{D}=\mathsf{R}^{-1}\begin{bmatrix}\mathbf{0}^{\mathsf{T}}\\ \frac{\lambda_w\rho D_2}{-\alpha e_{N+1}^T}\end{bmatrix}, \tag{34}$$

$\mathsf{r}_i\doteq r(r_i)$, as defined in (23), and $\mathbf{0}$ denotes the vector in $\mathbb{R}^{N+1}$ of all zeros. The last equality in (33) is because of the boundary conditions (2) and (3). Arranging the vectors $\overline{T}_j$ to obtain a long vector of all unknowns we get

$$\lambda_w\left(\rho^2\begin{bmatrix}T_{rr}(r_0,\theta_0)\\ \vdots\\ T_{rr}(r_n,\theta_0)\\ \vdots\\ T_{rr}(r_0,\theta_M)\\ \vdots\\ T_{rr}(r_n,\theta_M)\end{bmatrix}+\rho\begin{bmatrix}\frac{1}{r_0}T_r(r_0,\theta_0)\\ \vdots\\ \frac{1}{r_N}T_r(r_n,\theta_0)\\ \vdots\\ \frac{1}{r_0}T_r(r_0,\theta_n)\\ \vdots\\ \frac{1}{r_N}T_r(r_n,\theta_n)\end{bmatrix}\right)\approx\left(I_{N+1}\otimes\check{A}\right)\overline{T}-\mathbf{f} \tag{35}$$

where $\overline{T}$ contains all unknowns and $\otimes$ stands for Kronecker product and

$$\check{A}=-\rho\alpha\,d_Ne_{N+1}^{\mathsf{T}}+\lambda_w\rho^2D_1D_2,+\check{D}, \tag{36}$$

$$\mathbf{f}=[\mathbf{f}_1^t,\ldots\mathbf{f}_M^t]^t,\quad \mathbf{f}_j=\rho\,Q_jd_0-\rho\,\alpha T_{ex}\,d_N+\check{Q}_j. \tag{37}$$

Similarly, second order derivatives $T_{\theta\theta}(r_i,\theta_j)$ can be approximated using the corresponding $M\times M$ differentiation matrix $\mathcal{D}^{(2)}$ for periodic data. In such case it can be shown that the scaled vector of second order derivatives $\frac{\lambda_w}{r_i^2}T_{\theta\theta}(r_i,\theta_j)$ in all points of the grid can be approximated by

$$\lambda_w\begin{bmatrix}\frac{1}{r_0^2}T_{\theta\theta}(r_0,\theta_0)\\ \vdots\\ \frac{1}{r_N^2}T_{\theta\theta}(r_N,\theta_0)\\ \vdots\\ \frac{1}{r_0^2}T_{\theta\theta}(r_0,\theta_M)\\ \vdots\\ \frac{1}{r_N^2}T_{\theta\theta}(r_N,\theta_M)\end{bmatrix}\approx\lambda_w\left(\mathsf{R}^{-2}\otimes I_M\right)\left[\mathcal{D}^{(2)}\otimes I_{N+1}\right]\overline{T} \tag{38}$$

Neglecting discretization errors (35) and (38) yield a system of linear equations (the discrete forward problem) of the form

$$\widehat{\mathbf{A}}\mathbf{x}=\widehat{\mathbf{g}}, \tag{39}$$

where

$$\widehat{\mathbf{A}}=(I_{N+1}\otimes\check{A})+\lambda_w(\mathsf{R}^{-2}\otimes I_M)\left[\mathcal{D}^{(2)}\otimes I_{N+1}\right], \tag{40}$$

$$\widehat{\mathbf{g}}=\mathbf{f}-\mathbf{q},\quad \mathbf{q}=[\mathbf{q}_1^t,\ldots,\mathbf{q}_M^t]^t,\quad \mathbf{q}_j=[q_g(r_0,\theta_j),\ldots,q_g(r_N,\theta_j)]^t. \tag{41}$$

Thus, to calculate approximate solutions to the forward problem (1)–(3), the linear equation system (39) has to be solved.

4. Estimation approach

Since the solution to the discrete forward problem (39) depends on Q, the inverse estimation problem of $Q(\phi)$ can be formulated as a problem which consists in estimating a vector of parameters $\mathbf{Q}$ such that the difference between the temperatures $T(\mathbf{Q})$ and temperatures experimentally measured $\widetilde{T}$ on the outer wall of the tube is minimized in some sense. More precisely, following the notation of the previous section let $\mathbf{Q}^*=[Q_1^*,\ldots,Q_M^*]^t$ with $Q_j^*\doteq Q(\theta_j)$. The goal is to determine an estimate $\widetilde{\mathbf{Q}}$ for $\mathbf{Q}^*$ by solving the least squares problem

$$\widetilde{\mathbf{Q}}=\arg\min_{\mathbf{Q}\in\mathbb{R}^M}=\frac{1}{2}\|\mathbf{T}(\mathbf{Q})-\widetilde{\mathbf{T}}\|_2^2=\arg\min_{\mathbf{Q}\in\mathbb{R}^M}\frac{1}{2}\sum_{j=1}^{M}(T_j(\mathbf{Q})-\widetilde{T}_j)^2, \tag{42}$$

where $\mathbf{Q}$ is the vector of unknowns and $\mathbf{T}(\mathbf{Q})=[T_1(\mathbf{Q}),\ldots,T_M(\mathbf{Q})]^t$ is the vector of computed temperature values satisfying (39) at $r=r_N=1$ (or equivalently at $r=\mathsf{r}_E$). In order to determine such estimate, notice that the necessary condition for the vector $\widetilde{\mathbf{Q}}$ to be a minimum point is

$$\mathbf{J}^T(\mathbf{T}(\widetilde{\mathbf{Q}})-\widetilde{\mathbf{T}})=0, \tag{43}$$

where $\mathbf{J}$ is the so called sensitivity matrix with entries $[\mathbf{J}]_{i,j}=\frac{\partial T_i(\mathbf{Q})}{\partial Q_j}$. In addition, since the system matrix $\widehat{\mathbf{A}}$ does not depend on $\mathbf{Q}$, then

$$\widehat{\mathbf{A}}\frac{\partial\overline{T}(\mathbf{Q})}{\partial Q_j}=\frac{\partial\widehat{\mathbf{g}}(Q)}{\partial Q_j}\doteq\begin{bmatrix}0\\ \vdots\\ 0\\ (\rho\,d_0+R^{-1}e_1)\\ 0\\ \vdots\\ 0\end{bmatrix}j\text{th block} \tag{44}$$

and these partial derivatives also do not depend on $\mathbf{Q}$. Thus to determine the jth column of $\mathbf{J}$ it suffices to take the components of $\frac{\partial\overline{T}(\mathbf{Q})}{\partial Q_j}$ corresponding to the locations (r_N,θ_j). Another consequence of (44) is that second order derivatives of $\overline{T}(\mathbf{Q})$ with respect to Q_j vanish. From this observation together with Taylor Theorem around $\mathbf{Q}=0$ it follows that

$$\mathbf{T}(\widetilde{\mathbf{Q}})=\mathbf{T}(0)+\mathbf{J}\widetilde{\mathbf{Q}}. \tag{45}$$

From this and (43) it follows that $\widetilde{\mathbf{Q}}$ solves the normal equations

$$(\mathbf{J}^T\mathbf{J})\mathbf{Q}=\mathbf{J}^T\left[\mathbf{T}(0)-\widetilde{\mathbf{T}}\right].$$

Equivalently

$$\widetilde{\mathbf{Q}}=\arg\min_{\mathbf{Q}\in\mathbb{R}^M}\|\mathbf{J}\mathbf{Q}-(\mathbf{T}(0)-\widetilde{\mathbf{T}})\|_2^2. \tag{46}$$

However, despite the apparent simplicity in determining the above estimate, because the sensitivity matrix in inverse heat transfer problems is very ill-conditioned, some regularization method is required in order to filter out the contribution of noise in the solution.

4.1. Filtering via TSVD/TGSVD

Perhaps one of the most well-known methods to deal with ill-conditioned problems is truncated singular value decomposition (TSVD). TSVD is based on the SVD of $\mathbf{J}$ which reads

$$\mathbf{J}=\mathsf{U}\Sigma\mathsf{V}^T, \tag{47}$$

where $\mathsf{U} = [\mathsf{u}_1, \ldots, \mathsf{u}_N] \in \mathbb{R}^{N\times N}$ and $\mathsf{V} = [\mathsf{v}_1, \ldots, \mathsf{v}_N] \in \mathbb{R}^{N\times N}$ are orthogonal matrices and $\Sigma \in \mathbb{R}^{N\times N}$ is a diagonal matrix, $\Sigma = \mathrm{diag}(\sigma_1, \ldots, \sigma_N)$, with the singular values σ_j ordered such that $\sigma_1 \geqslant \cdots \geqslant \sigma_N \geqslant 0$. The naive least squares solution to (46) is thus given by

$$\widetilde{\mathbf{Q}} = \sum_{j=1}^{N} \frac{\mathsf{u}_j^t g}{\sigma_j} \mathsf{v}_j, \quad g = \mathbf{T}(0) - \widetilde{\mathbf{T}}. \tag{48}$$

Let $\mathbf{Q}^{\text{exact}}$ denote the solution to (46) corresponding to $g^{\text{exact}} = \mathbf{T}(0) - \mathbf{T}$, i.e., corresponding to the noiseless case. The main problem with $\widetilde{\mathbf{Q}}$ is that noise components in $\widetilde{\mathbf{T}}$ can be greatly amplified because of the division by small singular values; in this event the computed estimate $\widetilde{\mathbf{Q}}$ can differ enormously from $\mathbf{Q}^{\text{exact}}$. To filter out the contribution of noise to the computed solution, the Truncated SVD (TSVD) method determines regularized solutions by truncating the summation (48) to $k \leqslant N$ terms, see, e.g., [23]. Hence the kth TSVD solution is defined as

$$\mathbf{Q}_k = \sum_{j=1}^{k} \frac{\mathsf{u}_j^T g}{\sigma_j} \mathsf{v}_j, \quad k \leqslant N. \tag{49}$$

The point here is that if k is poorly chosen, the solution $\mathbf{Q}_k$ either captures not enough information about the problem or the noise in the data dominates the approximate solution. The challenge in connection with TSVD is thus how to choose a proper truncation parameter. Truncated GSVD solutions are defined similarly based on the GSVD of the matrix pair (A, L) where L is introduced to incorporate *a priori* information of the solution such as smoothness. The GSVD of (A, L) is a generalization of the SVD of A in the sense that the generalized singular values of (A, L) are the square roots of the generalized eigenvalue of the symmetric matrix pair (A^TA, L^TL) [21,23]. More explicitly, for $A \in \mathbb{R}^{M\times N}$ and $L \in \mathbb{R}^{p\times N}$, with $M \geqslant N \geqslant p$, which always occurs in discrete ill-posed problems, then the GSVD of the pair (A, L) reads

$$A = U \begin{pmatrix} S_1 & \mathbf{0} \\ 0 & I_{N-p} \end{pmatrix} X^{-1}, \quad V(S_2, \mathbf{0})X^{-1} \tag{50}$$

where $U = [u_1, \ldots, u_N] \in \mathbb{R}^{M\times N}$ and $V = [v_1, \ldots, v_p] \in \mathbb{R}^{p\times p}$ have orthonormal columns, $X = [\mathbf{x}_1, \ldots, \mathbf{x}_N] \in \mathbb{R}^{N\times N}$ is nonsingular, and $S_1 = \mathrm{diag}(\sigma_1, \ldots, \sigma_p)$ (with σ_i ordered in non increasing form), $S_2 = \mathrm{diag}(\mu_1, \ldots, \mu_p)$ (with μ_i ordered in nondecreasing form), are $p \times p$ diagonal matrices whose entries are positive and normalized so that

$$\sigma_i^2 + \mu_i^2 = 1.$$

The generalized singular values values of (A, L) are defined as the ratios

$$\gamma_i = \sigma_i / \mu_i. \tag{51}$$

Turning to the estimation of the heat-flux $Q(\phi)$, based on the GSVD of the matrix pair $(\mathbf{J}, L)$, a truncated GSVD solution is defined as

$$\mathbf{Q}_{k,L} = \sum_{i=p-k+1}^{p} \frac{u_i^T g}{\sigma_i} \mathbf{x}_i + \sum_{i=p+1}^{N} (u_i^T g)\mathbf{x}_i. \tag{52}$$

Obviously, the σ_i here has nothing to do with the "ordinary" singular value σ_i of $\mathbf{Q}$. The same observation holds for the vectors u_i. The challenge in connection with TGSVD is the same as that of TSVD: how to choose a proper truncation parameter.

4.1.1. Truncation parameter selection methods

In this work stable estimates of $\mathbf{Q}^*$ are computed by using truncated SVD equipped with two parameter selection criteria, namely the discrepancy principle (DP) by Morozov [26], which requires noise estimates of $\|\widetilde{\mathbf{T}} - \mathbf{T}\|_2$, and a criterion introduced recently by Bazán et al. [6] which does not require such information referred to as the minimum product rule (MPR). As usual we assume that "exact" data satisfies the discrete Picard condition, i.e., the coefficients $\mathsf{u}_j^t g$ decay in magnitude, on the average, faster than the singular values σ_i, until they level off at a plateau determined by the standard deviation of the noise. More precisely, if noise data are assumed such that $\widetilde{\mathbf{T}} = \mathbf{T} + \varepsilon$, with $\widetilde{\mathbf{T}}_j = \mathbf{T}_j + \varepsilon_j$, $j = 1, \ldots, N$, then there must exist a integer $\overline{k}$ such that

$$|\mathsf{u}_j^t g| = |\mathsf{u}_j^t g^{\text{exact}} + \mathsf{u}_j^t \varepsilon| \approx |\mathsf{u}_j^t \varepsilon|, \quad \text{for} \quad j > \overline{k}. \tag{53}$$

Index $\overline{k}$ marks the transition between decaying and flat coefficients $|\mathsf{u}_j^t g|$ and corresponds to a good balance between the regularized solution norm and the residual norm [23]. In addition, under the above assumptions it is known that the error $\|\mathbf{Q}^{\text{exact}} - \mathbf{Q}_k\|_2$ is minimized when $k = \overline{k}$ [10, Section 4.1]. A problem however is that index $\overline{k}$ is difficult to identify.

The truncation parameter chosen by DP is defined as the first k such that

$$\|R_k\|_2 \doteq \|\mathbf{J}\mathbf{Q}_k - g\|_2 \leqslant \tau\delta, \quad \delta = \|\widetilde{\mathbf{T}} - \mathbf{T}\|_2\|, \tag{54}$$

where $1 \lessapprox \tau$ is a user specified parameter. As for MPR, it chooses as truncation parameter the integer defined as

$$k_\psi = \arg\min \Psi_k, \quad \Psi_k = \|R_k\|_2 \|\mathbf{Q}_k\|_2, \quad k > 1. \tag{55}$$

Theoretical properties as well error bounds associated to DP are well established in literature and are therefore not included here. Regarding MPR, it appeared for the first time in connection with LSQR in [6] and more recently in connection with TSVD in [10]. DP and MPR are implemented similarly by considering the residual $R_{k,L}$ and corresponding TGVSD solutions $\mathbf{Q}_{k,L}$. Matlab m-files that implement TSVD and TGSVD are available in Hansen [24].

4.2. Filtering via Tikhonov regularization

Tikhonov regularization method (TRM) handles the ill-conditioning of the least squares problem (46) by determining regularized solutions defined by

$$\begin{aligned} \widetilde{\mathbf{Q}}_\lambda &= \arg\min_{\mathbf{Q}\in\mathbb{R}^M} \mathcal{F}_\lambda(\mathbf{Q}), \quad \mathcal{F}_\lambda(\mathbf{Q}) \\ &= \|\mathbf{J}\mathbf{Q} - (\mathbf{T}(0) - \widetilde{\mathbf{T}})\|_2^2 + \lambda^2 \|L\mathbf{Q}\|_2^2, \end{aligned} \tag{56}$$

where $\lambda > 0$ is the regularization parameter. $\mathcal{F}_\lambda(\mathbf{Q})$ represents a trade-off between two optimization processes: first, the fidelity of the fit and second, the smoothness or the stability of the solution. Thus, for the regularized solution $\mathbf{Q}_\lambda$ to be meaningful, the regularization parameter λ has to balance these two optimization processes. In other words, the choice of a good regularization parameter requires a good balance between the size of the residual norm and the size of the solution norm (seminorm when L has non trivial null space).

4.2.1. Regularization parameter selection methods

Perhaps one of most widely used regularization parameter choice methods is the L-curve (LC) method by Hansen and O'Leary [23]. The method determines the regularization parameter by locating the "corner" of the parametric curve in the (t, s) plane defined by

$$\begin{aligned} &\mathcal{L}: \ \{(t_\lambda, s_\lambda) \in \mathbb{R}^2, \ t_\lambda = \log(\|\mathbf{J}\mathbf{Q} - (\mathbf{T}(0) - \widetilde{\mathbf{T}})\|_2), \\ &s_\lambda = \log(\|L\mathbf{Q}\|_2), \ \lambda > 0.\} \end{aligned} \tag{57}$$

For ill-conditioned problems the curve $\mathcal{L}$ almost always has a well distinguished L-shaped appearance with distinctive vertical and

horizontal parts; when this is the case, the corner corresponds to a good balance between the size of the residual norm and the solution norm and the error in $\mathbf{Q}_\lambda$ with respect to $\mathbf{Q}^*$ tends to be within reasonable bounds. Computationally, the L-curve method selects the parameter which minimizes the curvature of $\mathcal{L}$, see Hansen and O'Leary [23]. In practice, the L-curve method has been proven to produce good regularization parameters in several cases. However, locating the corner in a robust way is not always an easy task, either because sometimes the curve displays several corners or because the corner is not visible at all. A method that has been proved to circumvent these difficulties on several test problems from the literature, is the fixed-point (FP) method and its variants proposed by Bazán and co-workers [3–5]. The fixed-point method requires computation of the solution seminorm and the corresponding residual norm, and selects the parameter which minimizes the product of these norms as a function of the regularization parameter. Like L-curve, the motivation to use this algorithm is that the sought minimizer corresponds to a good balance between the size of these norms. Algorithmically, the regularization parameter chosen by the fixed-point method is the limit value of the sequence

$$\lambda_{k+1} = \varphi(\lambda_k) = \frac{\|\mathbf{J}\mathbf{Q}_{\lambda_k} - (\mathbf{T}(0) - \widetilde{\mathbf{T}})\|_2}{\|L\mathbf{Q}_{\lambda_k}\|_2}, \quad k = 0, 1, \ldots \tag{58}$$

In practice, the sequence converges very quickly and the computed regularization parameter yields solutions with accuracy comparable to that of the L-curve method but it is more robust and less computational expensive [22,23]. Like the L-curve approach, the Fixed-point method does not require any *a priori* knowledge of the noise level. Another parameter choice rule that has gained relevance due to its theoretical properties is Morozov's discrepancy principle (DP) [26]. It suggests choosing the regularization parameter in such a way that the residual norm for the regularized solution $\mathbf{Q}_\lambda$ satisfies the non linear equation

$$\|\mathbf{J}\mathbf{Q}_\lambda - g\| = \tau\|\mathbf{e}\|, \tag{59}$$

where $\tau \gtrapprox 1$ is a user specified parameter and $\mathbf{e}$ denotes the data error: $\mathbf{e} = \tilde{g} - g_{\text{exact}} = \mathbf{T} - \widetilde{\mathbf{T}}$.

4.3. Filtering via differentiation matrix approach

When a thin wall pipe configuration is assumed to hold, that is, when $r_I \approx r_E$, the heat-flux distribution can be estimated by differencing the temperature distribution at the external tube wall as it can be explained shortly. Integrating (1) in $[r_I, r_E]$ gives

$$\lambda_w\left(r_E\frac{\partial T}{\partial r}(r_E,\theta) - r_I\frac{\partial T}{\partial r}(r_I,\theta)\right) = -\lambda_w\int_{r_I}^{r_E}\frac{1}{r}\frac{\partial^2 T}{\partial\theta^2}dr - \left[\frac{q_g r^2}{2}\right]_{r=r_I}^{r=r_E}. \tag{60}$$

Since $1/r$ does not change sign in the interval $[r_I, r_E]$, the weighted mean value theorem for integrals ensures that there exists $\hat{r}$ in $[r_I, r_E]$ such that

$$\int_{r_I}^{r_E}\frac{1}{r}\frac{\partial^2 T}{\partial\theta^2}dr = \frac{\partial^2 T}{\partial\theta^2}(\hat{r},\theta)\int_{r_I}^{r_E}\frac{1}{r}dr.$$

Inserting this result into (60), the boundary conditions (2) and (3) can be used to yield

$$r_E\alpha(T_{\text{env}} - T(r_E,\theta)) + r_I Q(\theta) = -\lambda_w\ln(r_E/r_I)\frac{\partial^2 T}{\partial\theta^2}(\hat{r},\theta) - \frac{q_g(r_E^2 - r_I^2)}{2}. \tag{61}$$

Thus

$$Q(\theta) = -\frac{1}{r_I}\left[\lambda_w\ln(r_E/r_I)\frac{\partial^2 T}{\partial\theta^2}(\hat{r},\theta) + \frac{q_g(r_E^2 - r_I^2)}{2} + r_E\alpha(T_{\text{env}} - T(r_E,\theta))\right] \tag{62}$$

and

$$h(\theta) = \frac{\lambda_w\ln(r_E/r_I)\frac{\partial^2 T}{\partial\theta^2}(\hat{r},\theta) + \frac{q_g(r_E^2 - r_I^2)}{2} + r_E\alpha(T_{\text{env}} - T(r_E,\theta))}{r_I(T_b - T(r_I,\theta))} \tag{63}$$

provided that $T(r_I,\theta) - T_b \neq 0$ for all $\theta \in [0, 2\pi]$. When $r_I \approx r_E$ it can be assumed that $T(r_I,\theta) \approx T(r_E,\theta)$ and $\frac{\partial^2 T}{\partial\theta^2}(\hat{r},\theta) \approx \frac{\partial^2 T}{\partial\theta^2}(r_E,\theta)$, in which case the heat-flux coefficient and the convective heat transfer coefficient can be estimated as

$$Q(\theta) \approx -\frac{1}{r_I}\left[\lambda_w\ln(r_E/r_I)\frac{\partial^2 T}{\partial\theta^2}(r_E,\theta) + \frac{q_g(r_E^2 - r_I^2)}{2} + r_E\alpha(t_{\text{env}} - T(r_E,\theta))\right] \tag{64}$$

and

$$h(\theta) \approx \frac{\lambda_w\ln(r_E/r_I)\frac{\partial^2 T}{\partial\theta^2}(r_E,\theta) + \frac{q_g(r_E^2 - r_I^2)}{2} + r_E\alpha(T_{\text{env}} - T(r_E,\theta))}{r_I(T_b - T(r_E,\theta))}. \tag{65}$$

Summarizing, to estimate the heat flux $Q(\theta)$ (hence $h(\theta)$), the second order derivative of measured temperature at the external tube wall has to be computed. The main difficulty here is that such computation is difficult because the available data are noise corrupted and because the noise tends to be amplified when the ill-posedness of the problem is not taken into account.

It is worth noticing that estimate (65) was derived differently by Bozolli et al. in [13], in which second order derivatives are calculated after the data is preprocessed in order to filter out high-frequency signal components through a Gaussian filter. In this section, an alternative technique to calculate second order derivatives is introduced in which such pre-processing step is avoided. The technique introduced here, which will be referred to as the filtering differentiation matrix approach (FDMA), is motivated by the observation that the eigenvalue problem

$$\begin{cases} y(x)'' + \lambda y(x) = 0, \ 0 < x < 2\pi, \\ y(0) = y(2\pi), \ y'(0) = y'(2\pi), \end{cases} \tag{66}$$

has as solution

$$\begin{cases} \lambda_0 = 0, \ \lambda_n = n^2, \ n = 1, 2, \ldots, \\ \gamma_0 = \text{cte}, \ \gamma_n(x) = \cos(nx), \ \zeta_n(x) = \sin(nx), \end{cases} \tag{67}$$

Interesting enough, when algebraic eigenvalue problems are used to approximate continuous eigen pairs of (66), the matrices involved in such approximation can be regarded as differentiation matrix operators. For example, using centered finite differences with meshspacing $h = 2\pi/N$, continuous eigen pairs (67) can be approximated by eigen pairs of the algebraic $N \times N$ eigenvalue problem with matrix defined by

$$\mathrm{D}^{(2)} = \frac{1}{h^2}\begin{bmatrix} -2 & 1 & & & 1 \\ 1 & -2 & 1 & & \\ & \ddots & \ddots & \ddots & \\ & & 1 & -2 & 1 \\ 1 & & & 1 & -2 \end{bmatrix}, \tag{68}$$

while second order derivative of $y(x)$ at grid points $x_i = ih$, $i = 1, \ldots, N$, can be approximated by the matrix vector product $\mathrm{D}^{(2)}\mathrm{y}$, with $\mathrm{y} = [y(x_1), \ldots, y(x_N)]^T$. It is noteworthy that $\mathrm{D}^{(2)}$ is singular and that its non zero eigenvalues can be proved to be negative. Obviously, a similar effect can be produced when using the second order Fourier differentiation matrix $\mathcal{D}^{(2)}$ introduced in the previous section.

The fact that discrete eigen pairs can be used as approximations to continuous eigen pairs is illustrated in Fig. 2 for $\mathrm{D}^{(2)}$ of size $N = 256$. The role of $\mathrm{D}^{(2)}$ as discrete differentiation operator is

illustrated in Fig. 3 for a discrete periodic function with and without noise.

Excellent quality results for the noiseless case is justified by the fact that the finite difference technique being used is second order accurate (in this case $\mathcal{O}(h^2) \approx \mathcal{O}\left(6 \times 10^{-4}\right)$). On the other hand, poor quality results in the noisy case can be explained by using the SVD of the discrete differentiation operator as follows. Let $\mathsf{D}^{(2)}$ have a SVD $\mathsf{D}^{(2)} = \mathsf{USV}^T$. Since $\mathsf{D}^{(2)}$ is Hermitian, its singular values and singular vectors are obtained immediately. More precisely, with the convention that singular are sorted in non decreasing order and that eigenvalues of $\mathsf{D}^{(2)}$ are presented in non increasing order, then $\sigma_1 = 0 \leqslant \sigma_2 \leqslant \cdots \leqslant \sigma_N$, $\sigma_i = -\lambda_i, \mathsf{v}_i = v_i$ and $\mathsf{u}_i = -\mathsf{v}_i$, with v_i being the eigenvector corresponding to λ_i. As a consequence, small singular values correspond to low-frequency eigenmodes while larger singular values correspond to high-frequency eigenmodes, as seen in Fig. 2. Thus, discrete second order derivatives $\widetilde{\mathsf{y}}''$ for noisy data $\widetilde{\mathsf{y}} = \mathsf{y} + \varepsilon$ with $\tilde{y}_i = y(x_i) + \epsilon_i,\ i = 1, \ldots, N$, becomes

$$\widetilde{\mathsf{y}}'' = \mathsf{D}^{(2)}\widetilde{\mathsf{y}} = \mathsf{USV}^T\widetilde{\mathsf{y}} = \sum_{i=1}^{N}\sigma_i\left(\mathsf{v}_i^T\widetilde{\mathsf{y}}\right)\mathsf{u}_i = \sum_{i=1}^{N}\sigma_i\left(\mathsf{v}_i^T\mathsf{y}\right)\mathsf{u}_i + \sum_{i=1}^{N}\sigma_i\left(\mathsf{v}_i^T\varepsilon\right)\mathsf{u}_i. \tag{69}$$

The second term in the right equality shows that the contribution of noise in the computed derivative will start dominating the final result when, for some i, $\sigma_i|\mathsf{v}_i^T\varepsilon| \gg 1$. Now, if noise is white, which means the magnitude of the Fourier coefficients $|\mathsf{v}_i^T\varepsilon|$ is approximately constant, because the singular values σ_i grow approximately as i^2, it follows that high-frequency components should start dominating the result very soon. Therefore, in order to filter out such components, the sum should be truncated soon as well. The same ideas can be implemented using the Fourier differentiation matrix or some other discrete differentiation operator.

Like TSVD, FDMA constructs approximate second order derivatives by truncating the sum in (69) to $k \leqslant N$ terms, giving rise to kth truncated second order derivatives defined by

$$\widetilde{\mathsf{y}}_k'' = \sum_{i=1}^{k}\sigma_i\left(\mathsf{v}_i^T\widetilde{\mathsf{y}}\right)\mathsf{u}_i. \tag{70}$$

Three kth truncated second order derivatives displayed in Fig. 4 show that while small values of k oversmooth the computed derivative, larger ones yield the opposite effect, and once again the challenge is how to choose a proper truncation parameter. The truncation parameter for FDMA will be determined by using the discrepancy principle (DP) and by MPR. To this end, considering (69) as the inverse solution to a linear problem of the form $Bs = \widetilde{\mathsf{y}}$ com $B = \mathsf{D}^{(2)^\dagger}$, it suffices to notice that the residual and solution norms associated to $\widetilde{\mathsf{y}}''^{(k)}$ are given as

$$\|\mathsf{R}_k\|_2^2 = \sum_{i=k+1}^{N}\left(\mathsf{v}_i^T\widetilde{\mathsf{y}}\right)^2, \quad \text{and} \quad \|\widetilde{\mathsf{y}}_k''\|_2^2 = \sum_{i=1}^{k}\sigma_i^2\left(\mathsf{v}_i^T\widetilde{\mathsf{y}}\right)^2. \tag{71}$$

With the above quantities at hand, the truncation parameter selection methods DP and MPR can be implemented as described in (54) and (55), respectively. Having determined the truncation parameter, say $\widehat{k}$, the reconstructed function can be calculated as

$$\mathsf{y}_{\widehat{k}} = \sum_{i=1}^{\widehat{k}}(\mathsf{v}_i^T\widetilde{\mathsf{y}})\mathsf{v}_i. \tag{72}$$

Reconstructed functions $\mathsf{y}_{\widehat{k}}$ and corresponding truncated second order derivatives determined by applying FDMA to the above data $\widetilde{\mathsf{y}}$ based on DP and MPR are displayed in Fig. 5. Parameter τ required to implement DP was chosen as $\tau = 1.1$. To asses the quality of computed quantities, a method that determines the smallest normwise relative error as a function of k was considered and denoted by OPT. Normwise relative errors reported in Table 1 show that both methods DP and MPR perform nicely and with errors relatively close to the optimum.

5. Numerical results

The main purpose of the section is to illustrate the performance of all estimation methods described before on two test problems, first, using synthetic data generated from the benchmark solution introduced in previous section, and second, using experimental data.

5.1. Synthetic data from benchmark solution

The test problem considered here generates temperature values from a benchmark solution introduced in (13) which takes into account physical quantities reported in [12] displayed in Table 2.

For the forward problem spatial derivatives are approximated using $n + 1 = 21$ Gauss–Lobatto points and derivatives with respect to θ are approximated with $N = 128$. High accuracy attributed to the pseudospectral approach in solving the forward problem is confirmed in Fig. 6.

For the inverse problem, $N = 128$ temperature values at the external tube wall are used:

$$\widetilde{\mathbf{T}}_j = T(\mathsf{r}_\mathrm{E}, \theta_j) + \varepsilon_j,\ j = 1, \ldots, 128, \tag{73}$$

with θ_j equally spaced on $[0\ 2\pi]$ and where ε_j are Gaussian random numbers scaled such that $\|\widetilde{\mathbf{T}} - \mathbf{T}\|_2/\|\mathbf{T}\|_2 = 2.5 \times 10^{-4}$, and $\delta = \|\widetilde{\mathbf{T}} - \mathbf{T}\|_2 = 0.86550$. Recall that the absolute error δ is required by DP as input data. Exact temperature values, noise corrupted temperature values, as well as the heat-flux coefficient estimated naively by solving the least squares problem (46) are displayed in Fig. 7. Poor quality results are explained by the fact that the sensitivity matrix is severely conditioned (in this case, $\mathrm{cond}(\mathbf{J}) = 1.0219 \times 10^{10}$). To prevent large variations of the heat-flux distribution when computing inverse solutions, a regularization matrix L is introduced in the estimation procedure; in this case, because the heat-flux is smooth, the regularization matrix is chosen to be a discrete second order differentiation operator defined by

$$L = \begin{bmatrix} 1 & -2 & 1 & & \\ & \ddots & \ddots & \ddots & \\ & & 1 & -2 & 1 \end{bmatrix}_{(N-2)\times N}. \tag{74}$$

Thus, all numerical results rely on the GSVD of the matrix pair $(\mathbf{J}, L)$.

5.1.1. TGSVD-based results

To describe results obtained by TGSVD, first notice from Fig. 8 that the parameter selection rules DP and MPR point out truncation parameters $k = 5$ for DP and $k = 3$ for MPR. The resulting regularized solutions $\mathbf{Q}_{5,L}$ and $\mathbf{Q}_{3,L}$ are displayed on the left of Fig. 9. Notice that $Q(\theta)$ and the estimated regularized solutions are close to each other. Estimates of the heat transfer coefficient $h(\theta)$ based on (5) and the estimated heat flux coefficient $Q(\theta)$, as well as the corresponding pointwise relative errors are also displayed in Fig. 9. The error distribution shows that both parameter truncation rules perform well, thereby confirming the effectiveness of MPR as already seen in other applications, e.g., [6].

5.1.2. Tikhonov regularization-based results

To describe results obtained by Tikhonov regularization, first notice that regularization parameters obtained with DP, FP and

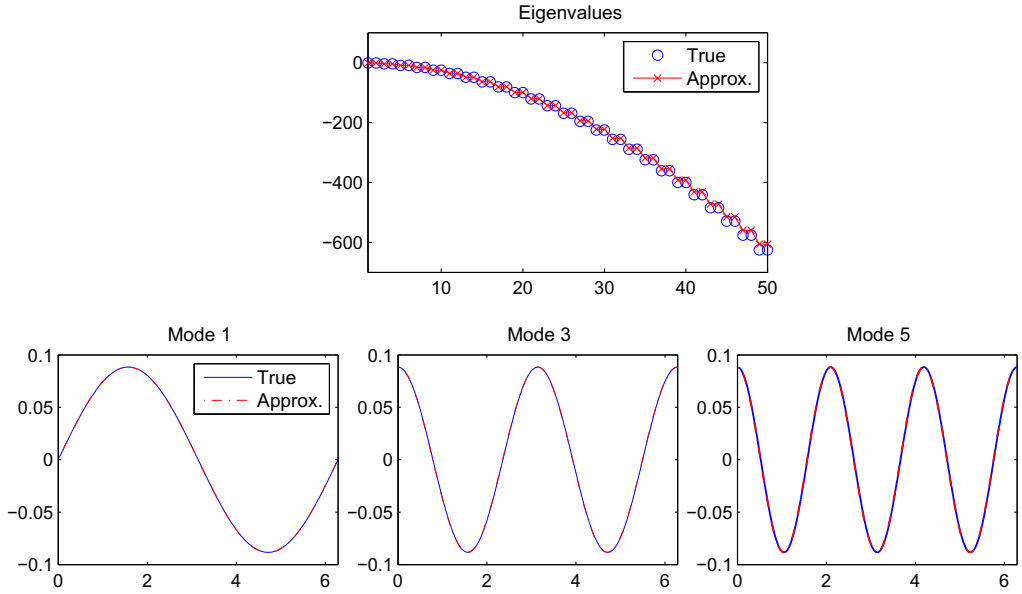

Fig. 2. Continuous and discrete eigen pairs of second order differentiation operator.

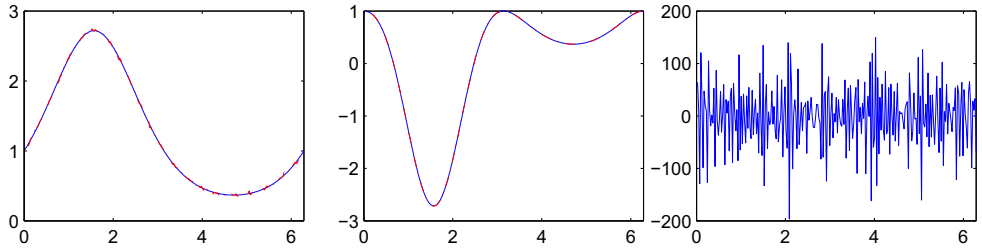

Fig. 3. Left: periodic data with and without noise. Middle: exact second order derivative and its approximation via matrix $D^{(2)}$ using noiseless data. Right: discrete second order derivative via matrix $D^{(2)}$ using noisy data.

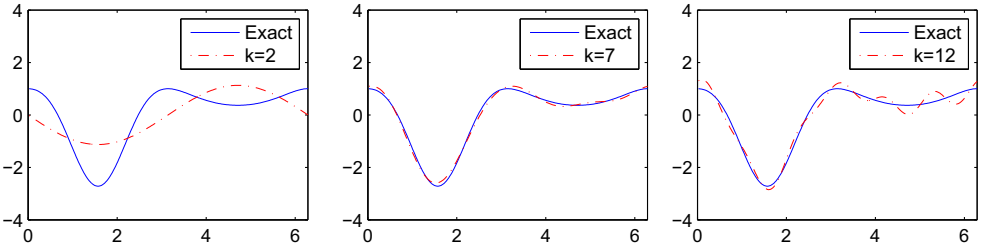

Fig. 4. Truncated second order derivatives using noisy data such that $\tilde{y} = y + 0.01\|y\|_2$. Exact data are generated by sampling the periodic function $y(x) = e^{\sin(x)}$.

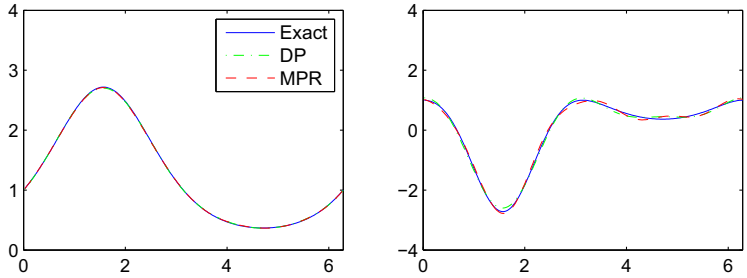

Fig. 5. Filtered data (left) and second order derivatives (right) obtained with FDMA based on DP and MPR as parameter choice rules with data described in Fig. 4.

Table 1
Truncation parameters and normwise relative errors.

	k	Error in $\bar{y}_k''$	Error in y_k
DP	7	0.0556	0.0042
MPR	11	0.0551	0.0038
OPT	9	0.0158	0.0034

Table 2
Physical quantities.

λ_w	α	q_g	T_b	T_{env}	r_I	r_E
15	5	4.8×10^6	295.2	294.2	0.012	0.015

L-curve are displayed in Fig. 10 using small circles. It is worth emphasizing that while DP requires knowledge of the noise level, FP and L-curve do not. Regularized solutions obtained with the computed parameters as well as the corresponding pointwise relative errors are all displayed in Fig. 11. The results confirm common experience regarding L-curve method in the sense that when the L-curve plot does not display multiple corners, FP, L-curve and DP perform generally well. Errors associated to the reconstructions of the heat transfer coefficient were approximately the same as those obtained via TGSVD (Fig. 9-right); for this they are not displayed here.

5.1.3. Filtered differentiation matrix-based results

Temperature data of the above numerical experiments are now used to illustrate how FDMA performs in recovering both the heat flux distribution and the heat transfer coefficient, concentrating on assessing the quality of inverse solutions as the tube thickness varies. For this, the heat-flux distribution $Q(\theta)$ and the heat transfer coefficient $h(\theta)$ will be estimated for three distinct values of r_I, keeping the outer radius unchanged and fixed at $r_E = 0.015$. FDMA is implemented using the discrete second order differentiation operator D^2 introduced in (68) with DP and MPR as parameter truncation rules; to assess its potential average normwise relative errors of 20 realizations are computed, which are denoted here by E_Q and E_H, respectively. Numerical results reported in Table 3 show that while the reconstruction quality of the heat flux coefficient is remarkably good and rather independent of the inner radius, this does not happen with the estimated heat transfer coefficient whose quality deteriorates as the thickness tube grows. This

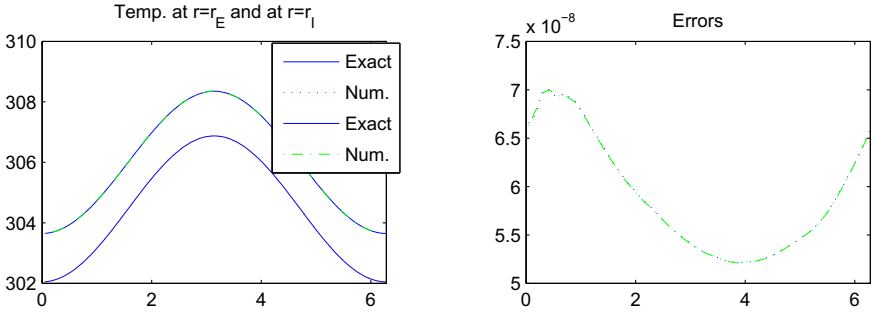

Fig. 6. Exact and computed temperatures by pseudospectral approach.

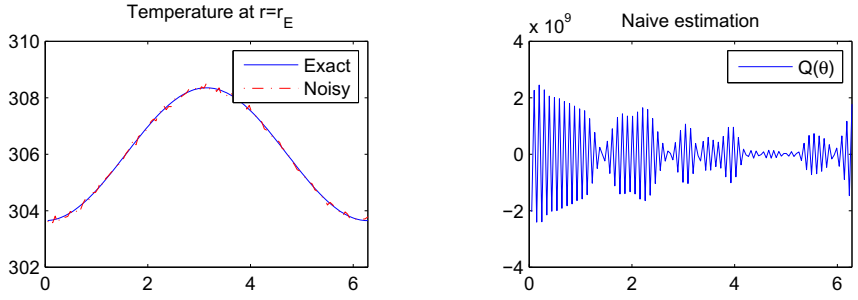

Fig. 7. Exact and noisy temperatures at the external tube wall, as well as the heat flux distribution $Q(\theta)$ naively estimated.

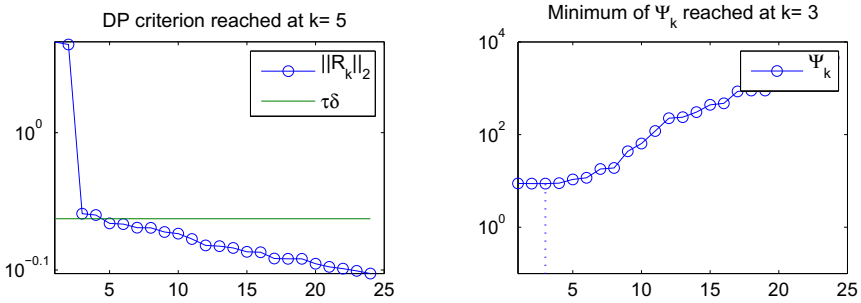

Fig. 8. Criteria DP and MPR.

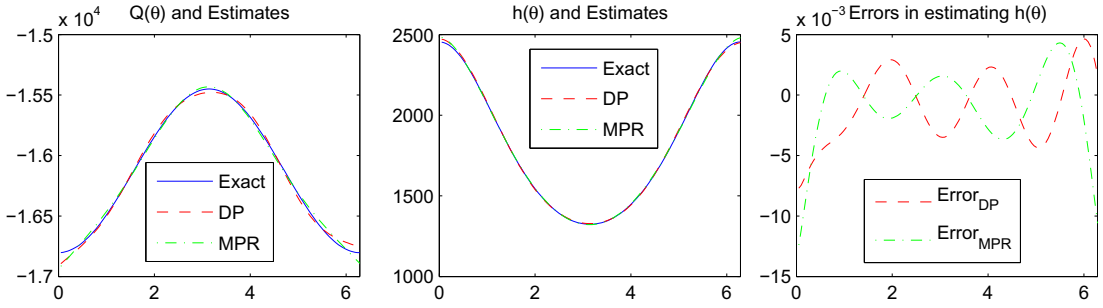

Fig. 9. Exact and estimated heat transfer coefficients and corresponding errors.

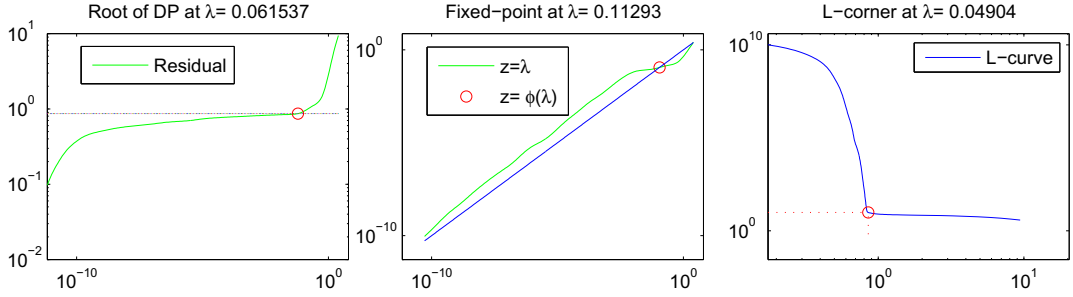

Fig. 10. Tikhonov regularization parameters determined by DP, FP and L-curve.

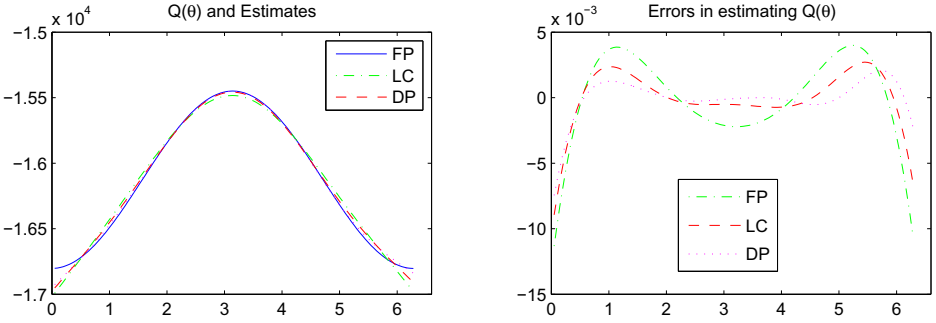

Fig. 11. Heat flux distribution $Q(\theta)$ and its estimates determined via Tikhonov regularization.

observation is illustrated in Fig. 12 with results obtained from the first realization.

More can be said to explain the poor quality of the estimated heat transfer coefficient for $r_1 = 0.012, 0.013$. Indeed, this behavior is due to the fact that FDMA is based on a simplified numerical model of the tube section, formulated by assuming thin wall approximation. This assumption is fully acceptable only when Biot number, defined as the product of convective heat transfer coefficient and tube thickness, divided by tube thermal conductivity, is smaller than 0.1 [8]. When the tube thickness becomes significant, the assumption is not fulfilled anymore and the thin wall approximation introduces important errors. In particular, for $r_1 = 0.014$ Biot number value is 0.04 while for $r_1 = 0.012$ it is 0.5 and the thin wall approximation is not acceptable. For illustration, Biot numbers associated to the above radii are shown in Table 4.

5.2. Quantifying performance of the methods

In order to complement the above results, the performance of all methods in estimating $Q(\theta)$and $h(\theta)$ from highly noisy data will now be assessed by computing relative errors in the reconstructed quantities. As before, noisy data $\widetilde{T}_j$ used in all numerical experiments are as in (73), but now with noise levels $\|\widetilde{\mathbf{T}} - \mathbf{T}\|_2 / \|\mathbf{T}\|_2 = \mathrm{NL} \times 10^{-2}$, with $\mathrm{NL} = 0.2, 0.4, 0.6, 0.8,$ and 1.0, i.e., noise levels 0.2%, 0.4%,...,1%. Since noise is random, average normwise relative errors, E_Q and E_H, of 20 instances were calculated for each noise level, with the observation that because L-curve failed constructing reasonable solutions several times, average value computation for LC was done using successful runs only: an LC-based solution was considered successful when the corresponding error did not exceed 0.5 (i.e. relative error 50%). In addition, since DP requires an upper bound on the noise level, see, (54) and (59), all computations involving DP were performed with $\tau = 1.1$ and the exact noise level as input data.

Errors in the reconstructions obtained with TGSVD and Tikhonov regularization are displayed in Fig. 13. Two aspects have to be emphasized. First, that the reconstruction quality is approximately the same for all methods, with a slight advantage in favor of MPR and LC, and second, that the reconstructions of the heat transfer coefficient are more sensitive than the reconstructions of the heat flux distribution. The reason for the increased sensitivity in estimating the heat transfer coefficient is explained by the fact

Table 3
Average normwise relative errors in estimating heath-flux distribution and heat-transfer coefficient from noisy data with noise level 0.025%.

	$r_I = 0.012$		$r_I = 0.013$		$r_I = 0.014$	
	DP	MPR	DP	MPR	DP	MPR
E_Q	0.3517×10^{-3}	0.5672×10^{-3}	0.2224×10^{-3}	0.6678×10^{-3}	0.2059×10^{-3}	0.4735×10^{-3}
E_H	0.1606	0.1606	0.0689	0.0688	0.0167	0.0167

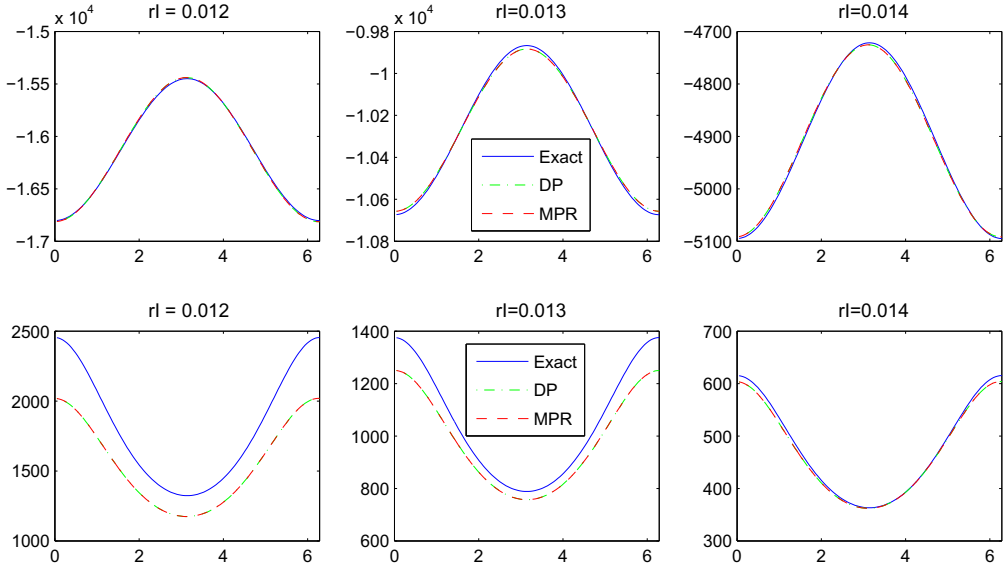

Fig. 12. Heat-flux distribution $Q(\theta)$ and heat-transfer coefficient $h(\theta)$ estimated by FDMA.

Table 4
Estimated Biot numbers Bi for three inner radii.

r_I	$s = r_E - r_I$	λ_w	h_{max}	$Bi = h_{max}s/\lambda_w$
0.012	0.003	15	2500	0.5
0.013	0.002	15	1400	0.1866
0.014	0.001	15	600	0.04

that the estimated temperature $\mathbf{T}(r_I, \theta)$ used to obtain the heat transfer coefficient in (5) incorporates two source of errors in the final result: the error in estimating $Q(\theta)$ and the error due to the forward solver.

Average relative errors obtained with FDMA are displayed in Fig. 14. The results show that the relative errors follow the same trend as those obtained in the case where the data are contaminated by low noise levels: the reconstruction quality of heat flux distributions is more accurate than that of the heat transfer coefficient, the latter depending strongly on the tube thickness. The reason for the decreased accuracy in estimating the heat-transfer coefficient is explained by the fact that such estimation depends on both the second order derivative of the measured temperature $\widetilde{\mathbf{T}}_j$, which is inaccurate, and the replacement of $\mathbf{T}(r_I, \theta)$ by an estimate that is obtained from the measured temperature, see Eqs. (63) and (65). (see Fig. 15).

The conclusion that can be drawn from Figs. 13 and 14 is that, except in the case when the tube thickness is very small, TGSVD and Tikhonov regularization produce more accurate solutions than FDMA.

5.3. Experimental data measured by infrared camera

In this section, all numerical estimation procedures will be tested using experimental data obtained in [12]. The data consist

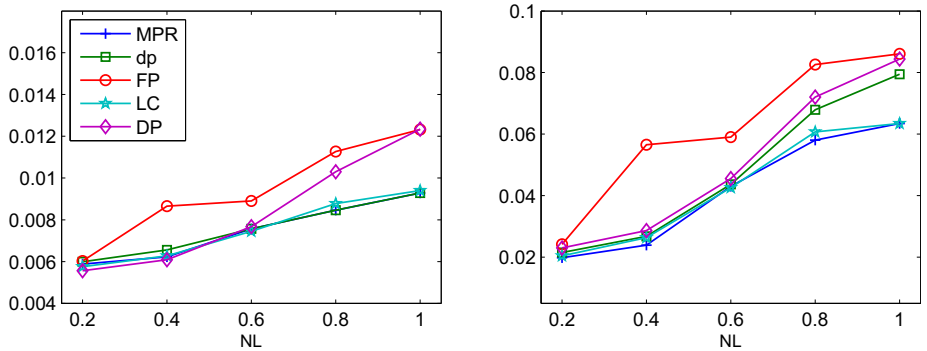

Fig. 13. Average normwise errors in estimating the heat flux Q (left) and the heat transfer coefficient $h(\theta)$ (right) by TGSVD and Tikhonov regularization for various noise levels.

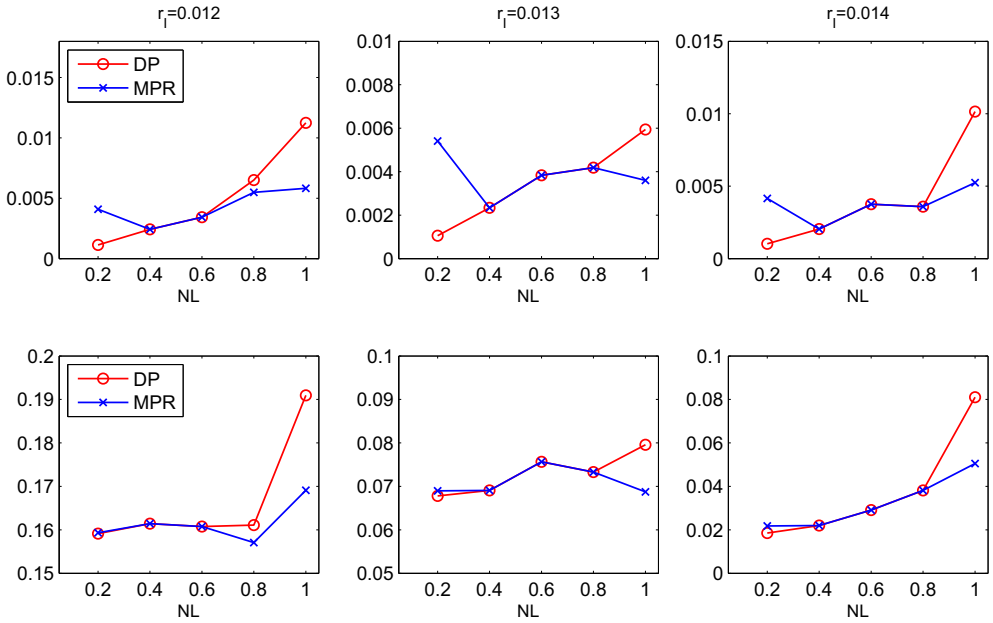

Fig. 14. Average normwise errors in estimating the heat-flux Q (top) and the heat-transfer coefficients (bottom) by FDMA for various noise levels and three distinct inner radius.

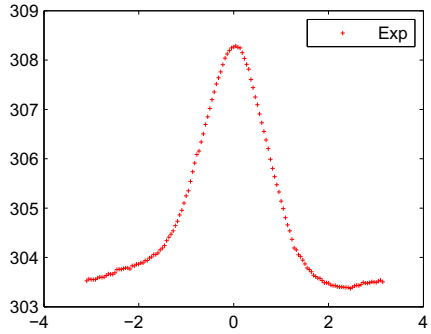

Fig. 15. Experimental data.

of 276 pointwise equality spaced temperature values acquired by a infrared camera on the exterior wall surface of a coiled tube, see Fig. 1. In this experimental investigation a stainless steel tube. The pipe under test was characterized by a helical profile composed by eight coils: the diameter and the pitch of the helix were of approximately 310 mm and 200 mm, respectively. The tube external diameter was equal to 16 mm with a 1 mm wall thickness. The surface temperature distribution was acquired experimentally by means of a FLIR SC7000 infrared camera, with a 640 × 512 pixel detector array. Its thermal sensitivity, as reported by the instrument manufacturer, is 20 mK at 303 K, while its accuracy is $\pm K$. Moving the infrared camera around the tube, different images of the test section were acquired: then thanks to a position reference fixed on the tube wall, the different infrared images were conveniently cropped, processed by perspective algorithms and merged together in Matlab environment. With this data processing procedure a continuous temperature distribution on the tube wall versus the circumferential angular coordinate was obtained. The heat transfer enhancement was investigated in laminar regime by using Ethylene Glycol as a working fluid. Except for the radii which were set to $r_I = 0.008$ and $r_E = 0.009$, the remaining system parameters are the same as in Table 2.

Again, to prevent large variations of the heat-flux distribution when computing inverse solutions, the second order discrete differentiation matrix L, see (74), is used as regularization matrix; hence, all estimated quantities rely on the GSVD of the matrix pair $(\mathbf{J}, L)$, where J is the sensitivity matrix. Also, since the data are experimental in nature and as the level of noise in the data is unknown, the choice of the regularization parameter through the discrepancy principle will not be used. The estimated heat flux distribution and corresponding heat transfer coefficient obtained

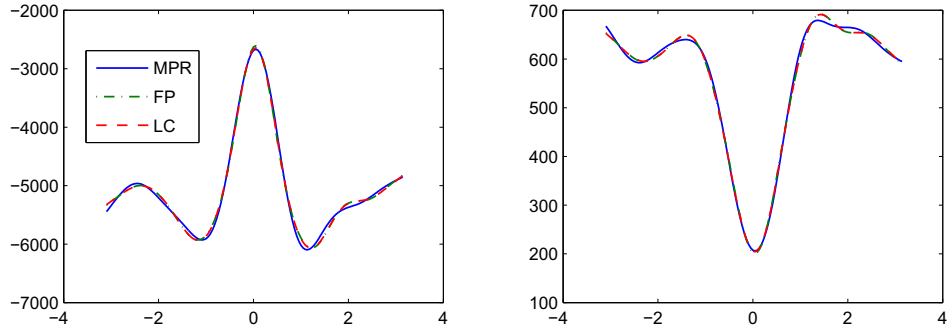

Fig. 16. Estimated heat flux distribution (left) and estimated heat transfer coefficient (right) both obtained by TGSVD and Tiknonov regularization from experimental measurements.

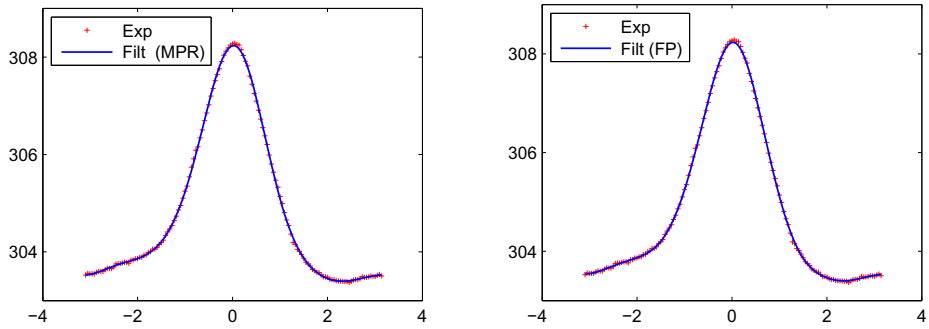

Fig. 17. Experimental data and filtered data.

through TGSVD and Tikhonov regularization are displayed in Fig. 16. The results obtained through FDMA are very similar and are not reported here. The results agree well with those obtained in [12] in which the forward problem is addressed using the finite element method available in Comsol Multiphysics, a commercial software.

The estimation methods are also able to filter out noise of the data after the heat flux distribution is available: by using (45) filtered temperature data can be computed as $\mathbf{T}_{\text{filtered}} = \mathbf{T}(0) + \mathbf{J}\mathbf{Q}(\cdot)$, where $\mathbf{Q}(\cdot)$ stands for the heat flux distribution obtained by regularization technique $(\cdot)$. Two temperature filtered data are displayed in Fig. 17, one based on TGSVD and the other one based on Tikhonov regularization.

6. Conclusions

In this work, several regularization methods for estimating the local convective heat transfer coefficient in coiled tubes have been proposed and assessed. The methods include truncated generalized singular value decomposition (TGSVD), Tikhonov regularization method (TRM), and a novel technique which truncates the frequency content of a discrete differentiation operator (FMDA) in order to filter out noise from data. Numerous numerical results on synthetic and experimental data have shown that the methods yield satisfactory results even when the data are highly contaminated by noise. Synthetic data used in the experiments resemble well experimental data often encountered in technical applications and may be useful in the assessment of numerical methods and in the design of coiled tube heat exchangers. Two factors contributed to the success of the methods: an efficient solver for the forward problem based on a highly accurate pseudospectral method and a proper selection of regularization parameters. Finally, since estimation errors in heat transfer coefficient depend on two source of errors, namely, input data errors and errors in heat flux distribution, non linear estimation techniques should be implemented in order to mitigate such dependence. This is the subject of ongoing work.

References

[1] O.M. Alifanov, Inverse Heat Transfer Problem, Springer, Berlin, 1994.
[2] B. Bai, L. Guo, Z. Feng, X. Chen, Turbulent heat transfer in a horizontal helically coiled tube, Heat Transfer-Asian Res. 28 (5) (1999) 395–403.
[3] F.S.V. Bazán, Fixed-point iterations in determining the Tikhonov regularization parameter, Inverse Prob. 24 (2008) 1–15.
[4] F.S.V. Bazán, J.B. Francisco, An improved Fixed-point algorithm for determining a Tikhonov regularization parameter, Inverse Prob. 25 (2009) 045007.
[5] F.S.V. Bazán, L.S. Borges, GKB-FP: an algorithm for large-scale discrete ill-posed problems, BIT Numer. Math. 50 (3) (2010) 481–507.
[6] F.S.V. Bazán, M.C.C. Cunha, L.S. Borges, Extension of GKB-FP algorithm to large-scale general-form Tikhonov regularization, Numer. Linear Algebra 21 (3) (2014) 316–339.
[7] A.E. Bergles, Techniques to enhance heat transfer, in: Handbook of Heat Transfer, McGraw-Hill, New-York, 1998.
[8] Th. L. Bergman, A.S. Lavine, F.P. Incropera, D.P. DeWitt, Fundamentals of Heat and Mass Transfer, John Wiley & Sons, 2011.
[9] J.V. Beck, B. Blackwell Jr., Ch.R. Clair, Inverse Heat Conduction – Ill-posed Problems, John Wiley& Sons Inc., New York, 1985.
[10] L.S. Borges, F.S.V. Bazán, M.C. Cunha, Automatic stopping rule for iterative methods in discrete ill-posed problems, Comput. Appl. Math. 34 (3) (2015) 1175–1197.
[11] F. Bozzoli, L. Cattani, S. Rainieri, F.S.V. Bazán, L.S. Borges, Estimation of the local heat transfer coefficient in coiled tubes: comparison between Tikhonov regularization method and Gaussian filtering technique, in: Proceeding of 14th International Conference on Inverse Problems in Engineering, Poland, 2014.
[12] F. Bozzoli, L. Cattani, S. Rainieri, F.S.V. Bazán, L.S. Borges, Estimation of the local heat-transfer coefficient in the laminar flow regime in coiled tubes by the Tikhonov regularisation method, Int. J. Heat Mass Transfer 72 (2014) 352–361.
[13] F. Bozzoli, L. Cattani, G. Pagliarini, S. Rainieri, Infrared image filtering applied to the restoration of the convective heat transfer coefficient distribution in coiled tubes, Opto-Electron. Rev. 23 (1) (2015) 109–117.
[14] F. Bozzoli, L. Cattani, S. Rainieri, G. Pagliarini, Estimation of local heat transfer coefficient in coiled tubes under inverse heat conduction problem approach, Exp. Therm. Fluid Sci. 59 (2014) 246–251.
[15] F. Bozzoli, G. Pagliarini, S. Rainieri, Experimental validation of the filtering technique approach applied to the restoration of the heat source field, Exp. Therm. Fluid Sci. 44 (2013) 858–867.
[16] H.T. Chen, X.Y. Wu, Estimation of heat transfer coefficient in two-dimensional inverse heat conduction problems, Numer. Heat Transfer Part B 50 (2006) 375–394.
[17] H.T. Chen, X.Y. Wu, Investigation of heat transfer coefficient in two-dimensional transient inverse heat conduction problems using the hybrid inverse scheme, Int. J. Numer. Methods Eng. 73 (2008) 107–122.
[18] D. Delpueyo, X. Balandraud, M. Grédiac, Heat source reconstruction from noisy temperature fields using an optimised derivative Gaussian filter, Infrared Phys. Technol. 60 (2013) 312–322.
[19] T.J. Martin, G.S. Dulikravich, Inverse determination of steady heat convection coefficient distributions, J. Heat Transfer 120 (1998) 328–334.
[20] B. Fornberg, A Practical Guide to Pseudospectral Methods, Cambridge University Press, Cambridge, 1996.
[21] G.H. Golub, C.F. Van Loan, Matrix Computations, third ed., The Johns Hopkins University Press, London, 1989.
[22] R. Haberman, Elementary Applied Partial Differential Equations with Fourier Series and Boundary Value Problems, second ed., Prentice Hall, Englewoods Cliffs, New Jersey, 1987.
[23] P.C. Hansen, Rank-Deficient and Discrete Ill-Posed Problems, SIAM, Philadelphia, 1998.
[24] P.C. Hansen, Regularization Tools: A MATLAB package for analysis and solution of discrete ill-posed problems, Numer. Algebra 6 (1994) 1–35.
[25] T. Lu, B. Liu, P.X. Jiang, Inverse estimation of the inner wall temperature fluctuations in a pipe elbow, Appl. Therm. Eng. 31 (2011) 1976–1982.
[26] V.A. Morozov, Regularization Methods for Solving Incorrectly Posed Problems, Springer-Verlag, New York, 1984.
[27] H. Massard, H.R.B. Orlande, O. Fudym, Estimation of position-dependent transient heat source with the Kalman filter, Inverse Prob. Sci. Eng. 20 (7) (2012) 1079–1099.
[28] H.R.B. Orlande, O. Fudym, D. Maillet, Thermal Measurements and Inverse Techniques, CRC Press, Taylor & Francis Group, Boca Raton, 2011.
[29] M.N. Ozisik, H.R.B. Orlande, Inverse Heat Transfer, Taylor & Francis, New York, 2000.
[30] R. Peiret, Spectral Methods for Incompressible Viscous Flow, Springer, Heildeberg, 2002.
[31] S. Rainieri, F. Bozzoli, L. Cattani, G. Pagliarini, Compound convective heat transfer enhancement in helically coiled wall corrugated tubes, Int. J. Heat Mass Transfer 59 (2013) 353–362.
[32] S. Rainieri, F. Bozzoli, L. Schiavi, G. Pagliarini, Numerical analysis of convective heat transfer enhancement in swirl tubes, Int. J. Numer. Methods Heat Fluid Flow 21 (5) (2011) 559–571.

[33] T.T.M. Onyango, D.B. Ingham, D. Lesnic, M. Slodicka, Determination of a time-dependent heat transfer coefficient from non-standard boundary measurements, Math. Comput. Simul. 79 (2009) 1577–1584.
[34] P. Naphon, S. Wongwises, A review of flow and heat transfer characteristics in curved tubes, Renew. Sustain. Energy Rev. 10 (2006) 463–490.
[35] M.F. Pakdaman, M.A. Akhavan-Behabadi, P. Razi, An experimental investigation on thermo-physical properties and overall performance of MWCNT/heat transfer oil nanofluid flow inside vertical helically coiled tubes, Exp. Therm. Fluid Sci. 40 (2012) 103111.
[36] Y. Rouizi, D. Maillet, Y. Jannot, Fluid temperature distribution inside a flat mini-channel: semi-analytical wall transfer functions and estimation from temperatures of external faces, Int. J. Heat Mass Transfer 64 (2013) 331–342.
[37] J. Su, G.F. Hewitt, Inverse heat conduction problem of estimating time-varying heat transfer coefficient, Numer. Heat Transfer 45 (2004) 777–789.
[38] L.N. Trefethen, Spectral Methods in Matlab, SIAM, Philadelphia, PA, 2000.
[39] J. Xu, T. Chen, A nonlinear solution of inverse heat conduction problem for obtaining the inner heat transfer coefficient, Heat Transfer Eng. 19 (1998) 45–53.
[40] J. Zhang, M.A. Delichatsios, Determination of the convective heat transfer coefficient in three-dimensional inverse heat conduction problems, Fire Saf. J. 44 (2009) 681–690.
[41] R. Zolfaghari, A. Shidfar, Restoration of the heat transfer coefficient from boundary measurements using the Sinc method, Comput. Appl. Math. 44 (2015). 34–29.